Chapter 3

Chemical Composition of Toluene and Cresol Secondary Organic Aerosol: Effect of NO Level[1]

---

[1] This chapter is reproduced by permission from "Chemical Composition of Toluene and Cresol Secondary Organic Aerosol: Effect of NO" by K. A. Schilling, H. Lignell, M. M. Coggon, R. H. Schwantes, X. Zhang, and J. H. Seinfeld. In submission to *Environmental Science and Technology*, 2015.

ABSTRACT

The NO_x effect on toluene SOA formation was studied under dry low- and high-NO conditions, and with varied seed: $(NH_4)_2SO_4$, Na_2SO_4, $MgSO_4$ + H_2SO_4, and NaCl. *o*-, *m*-, and *p*-Cresol SOA was produced under high-NO conditions to compare cresol and toluene SOA chemical compositions and assess the contribution of the cresol path to toluene SOA. Online aerosol mass spectrometry (HR-AMS, Aerodyne, Inc.) and offline direct analysis in real time mass spectrometry (DART-HR-MS, JEOL, Inc.) were used to chemically characterize SOA. Oxygenated compounds with general formulae $C_xH_yO_{5+}$ and $C_xH_yO_4$ together constitute a relative mass fraction > 0.9 of all toluene SOA components identified here. Oligomers are found to be important contributors to cresol-derived SOA (relative mass fractions: ortho, 0.13; meta, 0.03; para, 0.99). $C_{10}H_{10}O_4$ is the principal oligomeric species identified in toluene SOA formed under dry low-NO conditions, with a relative mass fraction of 3.0×10^{-5}. Under dry high-NO conditions, toluene SOA has a relative mass fraction of 0.99 $\geq C_7$ species, including $C_xH_yO_{5+}$, $C_xH_yO_4$, $C_xH_yNO_{5+}$, $C_xH_yNO_4$. A relative mass fraction of 0.84 of toluene SOA is estimated to be attributable to the cresol pathway, specifically $C_7H_8O_4$ (0.7) and $C_7H_6O_4$ (0.1) species, with the remainder composed of $C_xH_yO_2$, $C_xH_yNO_2$, $C_xH_yNO_3$, and C_xH_yO.

INTRODUCTION

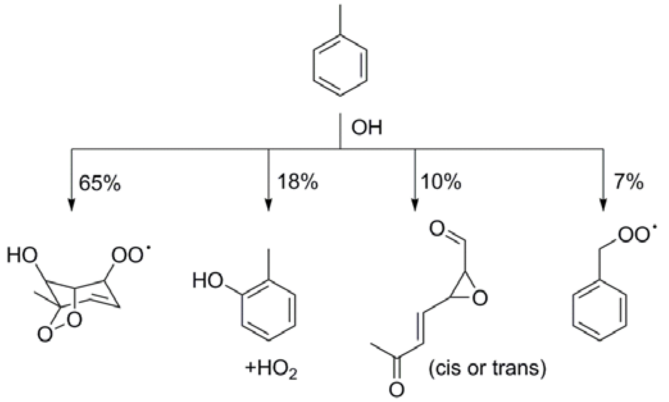

Figure 1. Gas-phase mechanism for toluene oxidation proceeding by OH addition, based on the Master Chemical Mechanism (MCM).[7]

Aromatic compounds are well-established precursors of secondary organic aerosol (SOA), and the gas-phase photooxidation chemistry of toluene and early aromatic oxidation products including cresol is the subject of numerous studies.[1-30] Toluene photooxidation occurs through four channels leading to the formation of bicyclic peroxy radicals, cresols, epoxy muconaldehydes, and peroxy methyl benzene radicals under low- and high-NO conditions (Fig. 1).[7] Here, we address toluene photooxidation by the major channels: the bicyclic peroxy radical and cresol pathways. Mechanisms for the minor pathways, taken from the Master Chemical Mechanism (MCM), are given in the Supporting Information.

Low- and extremely low-volatility compounds (LVOC and ELVOC) are of substantial interest in the study of SOA formation, and emerging technologies are enabling their detection.[31] Important related questions are the extent to which toluene and cresol SOA comprise LVOC and ELVOC, and the extent to which LVOC and ELVOC originate from multigenerational photooxidation and oligomerization under dry conditions. Oligomers, which include dimers up to polymers in excess of 500 amu, have been established as important compounds in aromatic SOA.[6, 28-29, 32-33] Glyoxal, a volatile oxidation product of aromatic compounds, can form oligomers in aromatic SOA, with its contribution related to the presence of particle-phase water.[26, 28] Hygroscopic seed and humid conditions facilitate partitioning of glyoxal to the particle phase.[26] In the present study, we expect minimal contributions from glyoxal to SOA growth due to the dry experimental conditions, and if oligomerization occurs, we anticipate other routes.

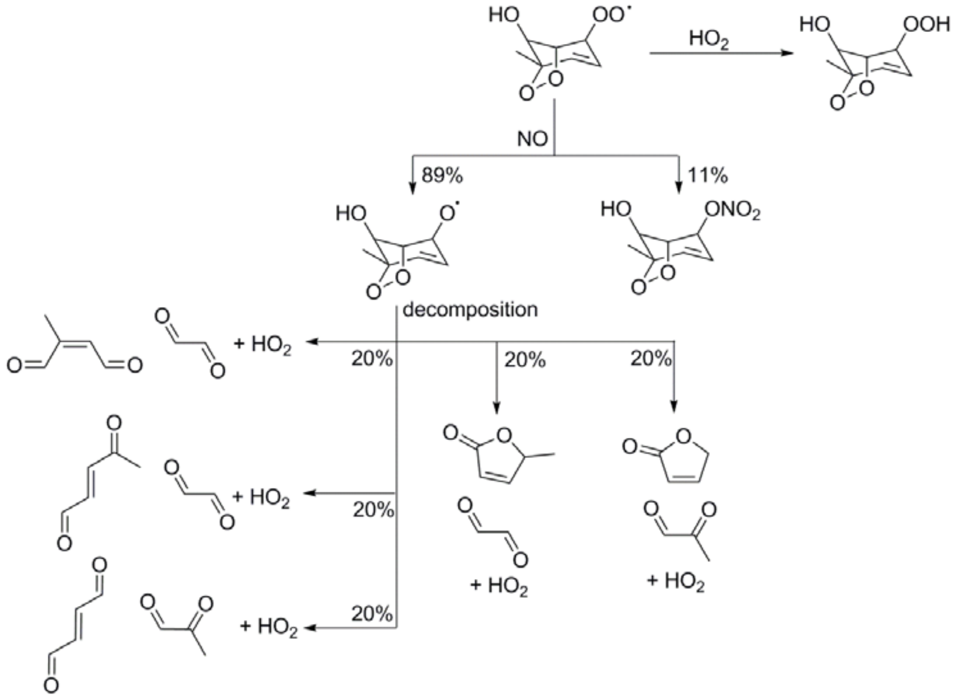

Figure 2. Mechanism for the gas-phase oxidation of the bicyclic peroxy radical under low- and high-NO conditions based on the Master Chemical Mechanism (MCM).[7]

The toluene-derived bicyclic peroxy radical pathway results primarily in ring-opening during decomposition of the bicyclic alkoxy radical formed from reaction with NO (Fig. 2). The decomposition products include unsaturated dicarbonyls of various chain lengths (e.g., glyoxal and methyl glyoxal), and lactones.[7] Symmetric species like glyoxal are capable of forming extensive oligomer networks, as linking groups are present on both ends of the molecule. Oligomers formed by dissimilar compounds may not span a large molecular weight range, as the monomers may not contain multiple functional groups capable of linking molecules. The bicyclic peroxy radical pathway can be considered a major contributor to toluene SOA when high concentrations of aldehydes and aldehyde-based oligomers are found in the particle phase, especially under humid conditions and with hygroscopic seed.

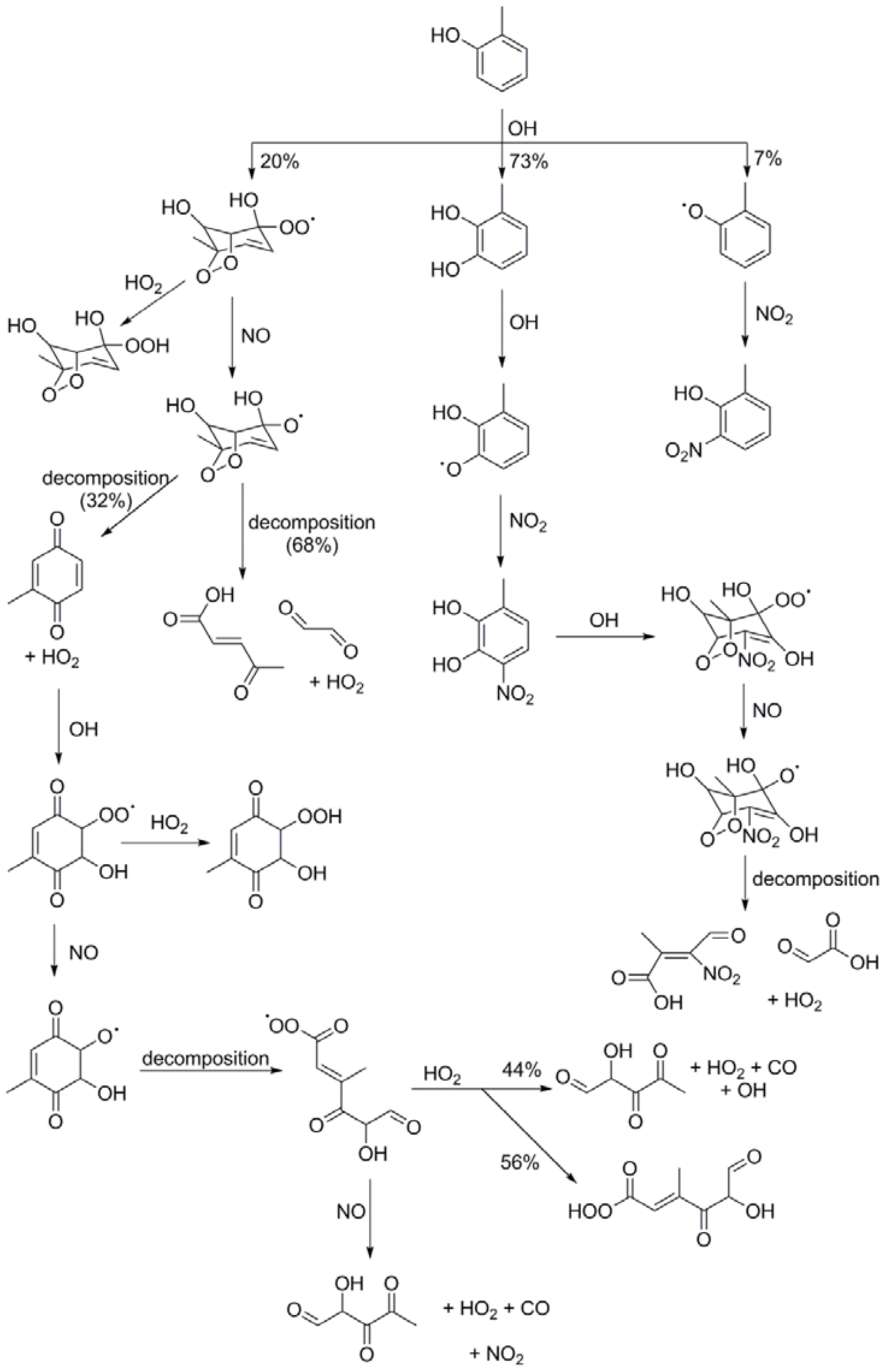

Figure 3. Gas-phase mechanism for *o*-cresol oxidation proceeding by OH addition, based on the Master Chemical Mechanism (MCM).[7]

The cresol pathway leads to its own bicyclic peroxy radical and polyhydroxylated toluene species which can retain the aromatic ring structure in subsequent oxidation steps or undergo a ring-opening step and decompose (Fig. 3). Methyl-*p*-benzoquinone is estimated to form at a 32% yield from the cresol-derived bicyclic alkoxy radical, and its continued oxidation produces both ring-retaining species and ring-opened products that form from alkoxy radical decomposition. These unsaturated carbonyl compounds can form lactones, furans, and oligomeric species, and resemble the later-stage products of toluene photooxidation along non-cresol channels. Unique chemical markers for the cresol pathway include ring-retaining polyhydroxylated and benzoquinone-based species, the presence of which demonstrates the relevance of the cresol pathway to toluene SOA chemical composition.

In this study, we characterize comprehensively toluene SOA composition by utilizing both online high-resolution aerosol time-of-flight mass spectrometry (HR-AMS) and offline direct analysis in real time high-resolution mass spectrometry (DART-HR-MS). We present chemical compositions for SOA produced by the photooxidation of toluene under low- and high-NO conditions in the presence of a variety of inorganic seeds: $(NH_4)_2SO_4$, Na_2SO_4, $MgSO_4$ + H_2SO_4, and NaCl. We also report the chemical composition of SOA from the photooxidation of *o*-, *m*-, and *p*-cresol under high-NO conditions with $(NH_4)_2SO_4$ seed aerosol. By producing and analyzing cresol-derived SOA under the same conditions as toluene SOA, we assess the role of cresol as an SOA precursor produced through the photooxidation of toluene. To assist in the comparison of the chemical composition of toluene and cresol SOA, we present results from the application of positive matrix factorization to the HR-AMS datasets for toluene and *o*-cresol high-NO SOA.

EXPERIMENTAL

Environmental Chamber Photooxidation Experiments

The hydroxyl radical-initiated photooxidation of toluene, *o*-, *m*-, and *p*-cresol produced SOA under low- and high-NO conditions in the dual California Institute of Technology environmental chambers, described elsewhere and in the Supporting Information (Table 1).[34-35] Low-NO conditions are defined here as NO mixing ratios < 5 ppb; high-NO conditions are defined as > 80 ppb NO. Seed composition was varied by using different inorganic salts: $(NH_4)_2SO_4$, Na_2SO_4, $MgSO_4$ + H_2SO_4, and NaCl. All cresol isomers were oxidized under similar high-NO and seed conditions to those of toluene to enable the comparison of the resulting SOA chemical compositions, thereby evaluating the contribution of the cresol pathway to toluene SOA formation. All experiments were conducted at 25.0 ± 0.5 °C and ≤ 3% relative humidity.

Table 1. Summary of Experimental Conditions.[a,b]

Code	Parent VOC	$[VOC]_0$ (ppb)	Oxidant Precursor	$[NO_x]_0$ (ppb)	Seed	Bulk O:C	Bulk H:C	Bulk N:C	Offline O:C	Offline H:C	Offline N:C
A	toluene	286	H_2O_2	ND	$(NH_4)_2SO_4$	0.78	1.34	0.00	0.71	1.14	2.4×10^{-11}
B	toluene	313	H_2O_2+NO	96	$(NH_4)_2SO_4$	0.81	1.26	0.04	0.60	1.21	0.07
C	toluene	295	H_2O_2+NO	103	Na_2SO_4	0.80	1.30	0.03	0.67	1.23	9.4×10^{-5}
D	toluene	290	H_2O_2+NO	102	$MgSO_4$+H_2SO_4	0.78	1.26	0.04	0.71	1.21	9.2×10^{-5}
E	toluene	319	H_2O_2+NO	91	NaCl	0.90	1.22	0.04	0.59	1.31	0.04
F	o-cresol	105	H_2O_2+NO	86	$(NH_4)_2SO_4$	0.89	1.15	0.05	0.65	1.00	1.2×10^{-4}
G	m-cresol	151	H_2O_2+NO	73	$(NH_4)_2SO_4$	0.73	1.19	0.03	0.86	1.99	4.1×10^{-7}
H	p-cresol	158	H_2O_2+NO	95	$(NH_4)_2SO_4$	0.92	1.21	0.04	0.88	1.75	7.7×10^{-7}

[a] ND = not detected. Limit of NO and NO_2 detection is 5 ppb. Limit of RH measurement is 3%. Bulk elemental ratios are derived from HR-AMS measurements. Uncertainty estimates for bulk O:C and H:C are 20% and 12%, respectively. Uncertainty estimates for bulk N:C ratios are not reported. Offline elemental ratios are derived from DART-HR-MS measurements.

[b] All ions of intensity ≥ 5% of the base peak in a DART-HR-MS mass spectrum are assigned a molecular formula. Background ions are not included.

Chemical Analysis of SOA by HR-AMS

Aerosol composition was recorded online using a high-resolution time-of-flight aerosol mass spectrometer (HR-AMS, Aerodyne Research, Inc.). The HR-AMS was operated switching every 1 min between the high-resolution W-mode and the lower-resolution, higher-sensitivity V-mode. The data were analyzed with Igor Pro (Wave Metrics, Inc.), utilizing the Squirrel 1.53G and PIKA 1.12G analysis toolkits. Air interference corrections were made to the fragmentation table by applying correction factors determined by in-line filter runs prior to the experiments.[36] Bulk SOA elemental composition was calculated following the methods and recommendations of Aiken *et al.* and Canagaratna *et al.*[36-37]

Positive matrix factorization analysis (PMF) was used to investigate qualitatively the differences in aerosol compositions between toluene and o-cresol SOA produced under high-NO conditions with $(NH_4)_2SO_4$ seed. A detailed description of PMF application to chamber HR-AMS data can be found in Craven *et al.*[38] Details of the PMF application procedure and support for the solutions presented here appear in the Supporting Information.

Chemical Analysis of SOA by DART-HR-MS

SOA was collected by filtration over the final 4 h of experiments at 24 L min^{-1} with a Teflon membrane filter (47 mm, 1.0 μm pore size, Pall Life Sciences) and analyzed by high-resolution direct analysis in real time mass spectrometry (DART-HR-MS, JEOL, Inc.). A DART source is a low-temperature He plasma that generates primarily pseudomolecular ($[M+H]^+$) ions in positive mode through proton transfer reactions between the analyte, M, and ionized ambient water vapor (H_3O^+).[39-40] Samples are introduced for analysis directly into the DART stream, between the end of the DART source and the mass spectrometer inlet. In this study, a portion of the filter membrane was cut free from the support ring using a clean stainless steel scalpel and wrapped in a spiral around the barrel of a clean glass Pasteur pipet. The pipet was rotated slowly in the DART stream to warm the glass and desorb organic material gently from the Teflon filter. Each sample was cut and analyzed in triplicate. Intrasample peak intensity variability was < 3%. Additional analysis details, mass spectra for each SOA sample, and tabulated interpreted mass spectral data corrected to remove background ions are provided in the Supporting Information.

The accurate m/z of each ion $\geq$ 5% of the base peak intensity was fit to a chemical formula, adjusted to its neutral form, and given a proposed structure based on MCM toluene photooxidation and previously reported components of toluene SOA.[1-5, 7, 12, 17, 19, 21, 23, 30, 41] The Estimation of Vapor Pressure of Organics, Accounting for Temperature, Intramolecular, and Non-additivity Effects (EVAPORATION) model was used for each proposed structure, given in Simplified Molecular-Input Line-Entry System (SMILES) notation, to estimate the vapor pressure of the compound.[42] The EVAPORATION model is compatible with molecules containing oxygen-based functional groups and nitrates. To fit within these parameters, the vapor pressures of species proposed to be imines and N-containing heterocycles were estimated by using their oxygenated equivalent, and the vapor pressures of compounds containing nitro groups were estimated by substituting with a nitrate group.

DART-generated ion signal intensity for a given species is proportional to its vapor pressure, proton affinity, and concentration.[43-44] Targeted quantitative DART-MS analysis is performed by co-analyzing a compound with its isotopically labeled counterpart. In broad-spectrum quantitative analyses, such as those in this study, an internal standard must be chosen within the expected range of proton affinities and vapor pressures. The application of a droplet of internal standard solution to filtered SOA may lead to undesirable side reactions and alteration of SOA composition. Dibutyl phthalate (DBP) was chosen as an internal standard, as it is found in the Teflon filters used in this study, and its proton affinity and vapor pressure are within the expected range of proton affinities and vapor pressures for toluene and cresol SOA components. DBP and typical SOA components have proton affinities that are estimated to be comparable, leading to an analyte: standard proton affinity ratio of approximately 1.[44] With a proton affinity ratio of 1, analyte concentrations relative to DBP were arrived at by multiplying the ratio of vapor pressure of DBP to the analyte vapor pressure predicted by EVAPORATION by the ratio of the intensity of the analyte pseudomolecular ion to the intensity of the DBP pseudomolecular ion. Mixing ratios, also called relative mass fractions here, were calculated by dividing an analyte or analyte class by the sum of all measured SOA compounds for that given sample. The maximum propagated uncertainty in relative mass fractions for all species, based on 3% intensity variation, is 3×10^{-14}; this uncertainty holds for all reported relative mass fractions. Weighted average values for elemental ratios from offline analysis results were obtained by summing the products of each species mixing ratio by the H:C, O:C, or N:C for each species molecular formula (Table 1).

RESULTS AND DISCUSSION

Quantitative Analysis of Toluene and o-, m-, and p-Cresol SOA

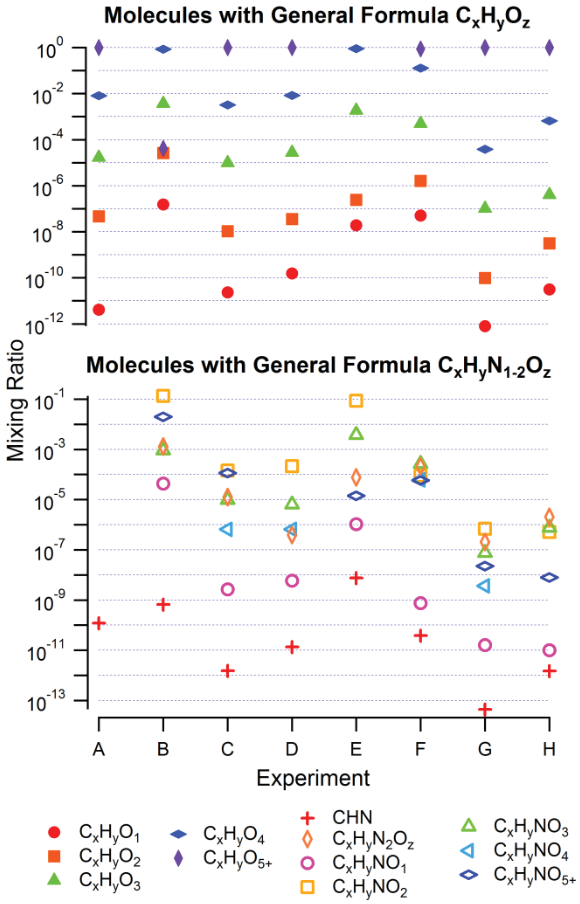

Figure 4. Chemical composition of SOA produced in current toluene and cresol photooxidation experiments as measured by offline DART-HR-MS analysis, displayed by general molecular formula category. Table 1 contains the key with experimental details.

The composition of both high- and low-NO SOA derived from toluene is dominated by species with the general formulae $C_xH_yO_{5+}$ and $C_xH_yO_4$, and N incorporation is significant only under high-NO conditions (Fig. 4). The SOA compositions reported here are consistent with multigenerational photooxidation through the bicyclic peroxy radical and cresol pathways as the primary routes to toluene SOA formation under low- and high-NO conditions. Toluene low-NO SOA does not feature significant N incorporation, indicating the expected lack of nitrate and nitro group formation as well as the inhibition of seed-related processes like imine formation, which can occur with high concentrations of carbonyls in the presence of ammonium sulfate (Table 1 and Fig. 4).[44] Pyridine formation, while minor, is ubiquitous in these experiments and potentially attributable to artifactual chemistry on the chamber walls (see Supporting Information).

Under high-NO conditions, the most highly oxygenated compounds ($C_xH_yO_{5+}$) constitute relative mass fractions of 0.99 for toluene- and cresol-derived SOA; no clear seed effect related to O number is observed. The next most abundant general molecular formulae are $C_xH_yO_4$ and $C_xH_yO_3$. $C_xH_yO_2$ compounds, including glyoxal, constitute $\leq 1\%$ by mass of toluene and *o*-, *m*-, and *p*-cresol SOA under these dry, high-NO conditions. The most abundant nitrogenous species are oxygenated nitro compounds or nitrates, $C_xH_yNO_{5+}$. The bulk N:C ratios for all high-NO SOA systems studied are consistent across seed types, supporting gas-phase reactions with NO to form nitrates and nitro compounds as the origins of the N functionality (Table 1). The difference between the bulk and offline N:C ratios can be attributed to uncertainty in the estimated vapor pressures of compounds with N-containing functional groups, which fall outside the present scope of the EVAPORATION model (e.g., imines, nitro groups). For broad-spectrum quantitation by DART-HR-MS, accurate vapor pressures are necessary.

Species found in *o*-cresol high-NO SOA constitute a relative mass fraction of 0.84 of toluene high-NO SOA in this study. $C_7H_8O_4$, interpreted as tetrahydroxytoluene (estimated vapor pressure 9.0×10^{-14} atm), comprises a relative mass fraction of 0.70 in toluene high-NO SOA. $C_7H_6O_4$, corresponding to trihydroxybenzaldehyde (estimated vapor pressure 8.3×10^{-9} atm) contributes a relative mass fraction of 0.10 to toluene high-NO SOA. $C_7H_6O_3$, proposed to be dihydroxybenzaldehyde, contributes a relative mass fraction of 2.5×10^{-5} to toluene high-NO SOA. The additional 0.04 is composed of molecules with general formulae $C_xH_yNO_2$, $C_xH_yNO_3$, C_xH_yO, and $C_xH_yO_2$ (see Supporting Information). The particle-phase measurement of modest concentrations of these moderate- to high-volatility oxidation products is attributed to the proposed trapping of condensing volatiles during the rapid accumulation of organic material in the growth phase.[45,46] Partial re-partitioning of volatile species occurs, possibly because the expected glassy nature of SOA may trap trace amounts of volatiles.

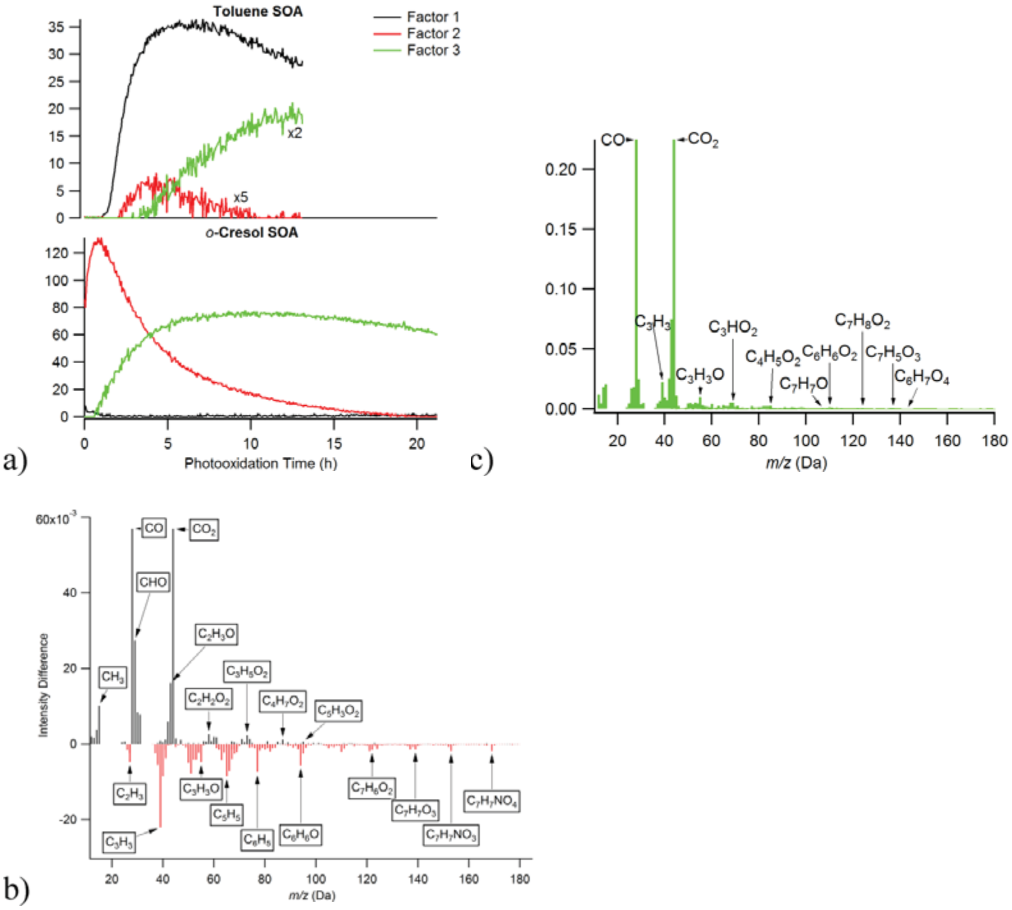

Figure 5. Three-factor PMF solution comparing toluene and *o*-cresol SOA produced under high-NO conditions in the presence of $(NH_4)_2SO_4$ seed. (a) Factor time trends: factor 1, distinct ions characterizing toluene SOA (black); factor 2, ions common to both toluene and cresol SOA related to early-generation cresol oxidation, multiplied by 5 for clarity (red); factor 3, ions from later-generation toluene and cresol oxidation (green), multiplied by 2 for clarity. (b) The difference between factor 1 (black) and factor 2 (red) mass spectral profiles. (c) Factor 3 mass spectral profile (green).

Detailed PMF analysis of the HR-AMS spectra of toluene and cresol SOA was conducted to assess qualitatively the chemical pathways leading to SOA formation under high-NO conditions. A three-factor fit is the simplest solution that captures the variation of the HR-AMS data within the known uncertainties of HR-AMS spectra (Fig. 5a). Toluene high-NO SOA has a distinctive factor (factor 1, shown in black); this is expected, given that no toluene is present in the cresol experiment. A shared factor (factor 2) describes early-generation *o*-cresol high-NO SOA and a small fraction of toluene high-NO SOA. The later, gradual decrease of factor 2 can be attributed to partial repartitioning of higher-volatility early-stage oxidation products back to the gas phase. Another shared factor (factor 3) describes the later-generation high-NO toluene and *o*-cresol SOA. Figure 5b shows the difference spectrum obtained by subtracting the mass spectral profile of factor 1 from that of factor 2. The difference spectrum shows enrichment in the unique toluene SOA profile (factor 1) of marker ions for highly oxidized species (e.g. CO_2^+) and unsaturated ketones and aldehydes (e.g., $C_2H_2O_2^+$, $C_4H_7O_2^+$, $C_3H_5O_2^+$, $C_5H_3O_2^+$). Marker ions for ring-retaining aromatic oxidized species (e.g. $C_3H_3^+$, $C_7H_7O_3^+$, $C_6H_6O_2^+$) are observed in early generation *o*-cresol SOA (factor 2). Factor 3 describes the late stages of multigenerational photooxidation, in which toluene and *o*-cresol SOA compositions converge, and features marker ions for aromatic ring-retaining oxidation products (e.g., $C_7H_8O_2^+$, $C_7H_8O_2^+$, $C_6H_7O_4^+$) (Fig. 5c). The measurement of a family of shared chemical species is expected based on the MCM for toluene and cresol photooxidation (Figs. 1-3).

Elemental Ratios as Descriptor of Toluene and Cresol Chemical Composition

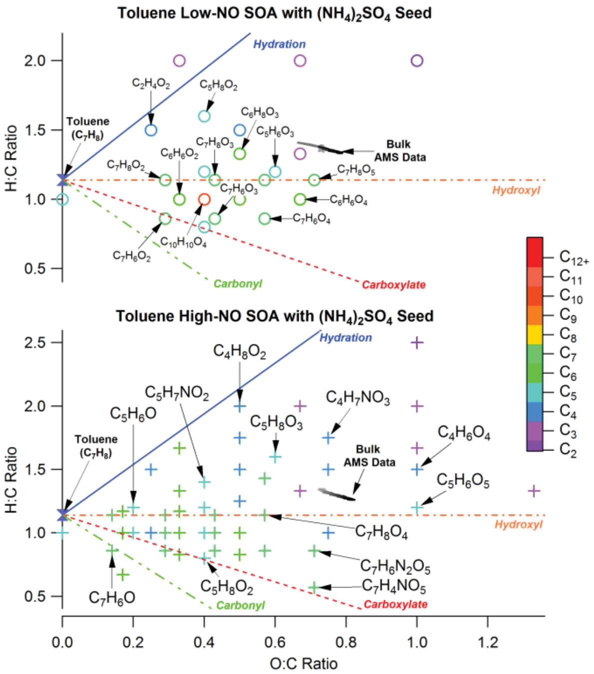

Figure 6. Species identified by DART-HR-MS analysis in the present study of toluene SOA produced under low- and high-NO conditions with $(NH_4)_2SO_4$ seed are displayed in van Krevelen space. Data markers are colored by the molecular formula C number. The bulk H:C and O:C elemental ratios derived from HR-AMS measurements are shown in grayscale for both low-NO and high-NO conditions.

Van Krevelen diagrams depict concisely variations in the functionalization of a complex organic mixture.[47-49] Figure 6 displays in van Krevelen space the elemental ratios for species measured by DART-HR-MS in the present study of toluene SOA generated under dry, low-, and high-NO conditions in the presence of $(NH_4)_2SO_4$ seed aerosol. Lines representing various functionalization pathways are shown. Not all measured species have a unique coordinate in van Krevelen space, as redundancies in H:C and O:C ratios may occur with nitrogen incorporation.

Multigenerational oxidation chemistry is evident in the polyfunctional species measured in these experiments. The majority of compounds in both high- and low-NO toluene SOA are C_7: $C_7H_8O_4$ in high-NO conditions and $C_7H_8O_5$ under low-NO conditions. These formulae are consistent with tetra- and pentahydroxytoluene, which are suggestive of oxidation following the cresol pathway.

Toluene high-NO SOA in this study is also characterized by < C_7 compounds, which are attributed to decomposition of toluene- and cresol-derived bicyclic peroxide intermediates (Fig. 2, 3, 6). Carboxylate formation (or the equivalent addition of carbonyl and hydroxyl groups on different sites within the same molecule) occurs on C_7 and C_5 backbones in toluene SOA, supporting the contribution from ring-opening non-cresol pathways (72% yield, by MCM). Bulk SOA H:C and O:C HR-AMS data have a slope of -2, supporting the relevance of carbonyl functionalization to toluene SOA formation under both low- and high- NO conditions.

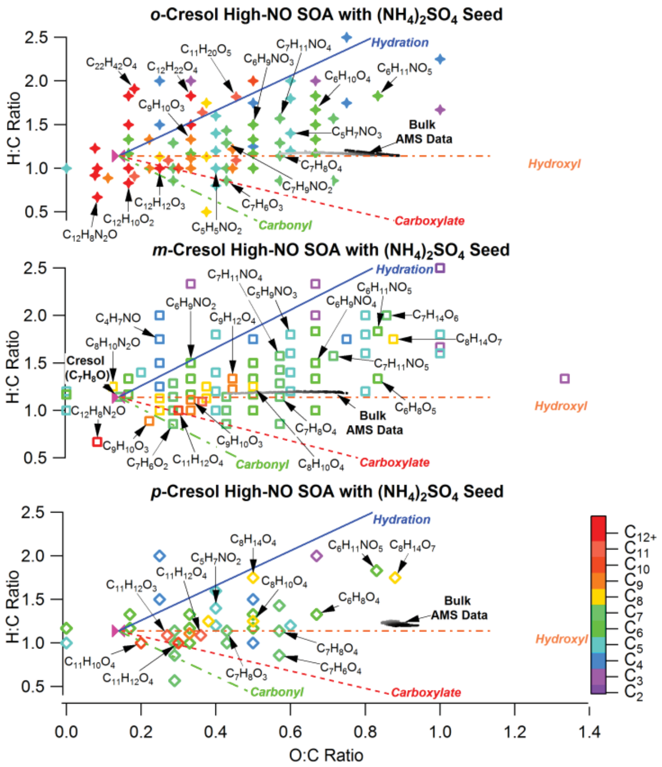

Figure 7. Van Krevelen diagram depicting chemical compositions of cresol SOA produced under high-NO conditions with $(NH_4)_2SO_4$ seed, as measured by offline DART-HR-MS. Data markers are colored by the molecular formula C number. The bulk SOA H:C and O:C elemental ratios derived from HR-AMS measurements are shown in grayscale.

Figure 7 displays the chemical composition of individual *o*-, *m*-, and *p*-cresol SOA formed under high-NO conditions with $(NH_4)_2SO_4$ seed. *o*- and *m*-Cresol SOA span a much larger O:C range than *p*-cresol SOA does, yet the final bulk O:C and H:C values for all three cresol isomers are similar

(Table 1). The close proximity of the electron-rich hydroxyl group to the methyl group in *o*- and *m*-cresol may affect ring-opening pathways and further functionalization in ways that do not occur for *p*-cresol.

Both offline and online SOA chemical characterization suggest repeated hydroxylation is an important process for SOA formation from all cresol isomers (Fig. 7). This finding is consistent with the MCM-estimated 73% of cresol undergoing further OH addition (Fig. 3). The majority of SOA mass for all cresol isomers is attributable to C_{7-10} compounds; oligomerization through hemiacetal formation from C_7 compounds and small carbonyl species may be the source of these products. Increased H:C ratios and decreased C number are consistent with the expected decomposition products of the bicyclic alkoxy radical formed from continued high-NO photooxidation of cresol. These unsaturated oxidized species are measured as monomeric and oligomeric species, ranging from C_5 to C_{11} in chain size, and in the case of *o*-cresol up to C_{22}.

Species Carbon Number as a Descriptor of Toluene and Cresol SOA Composition

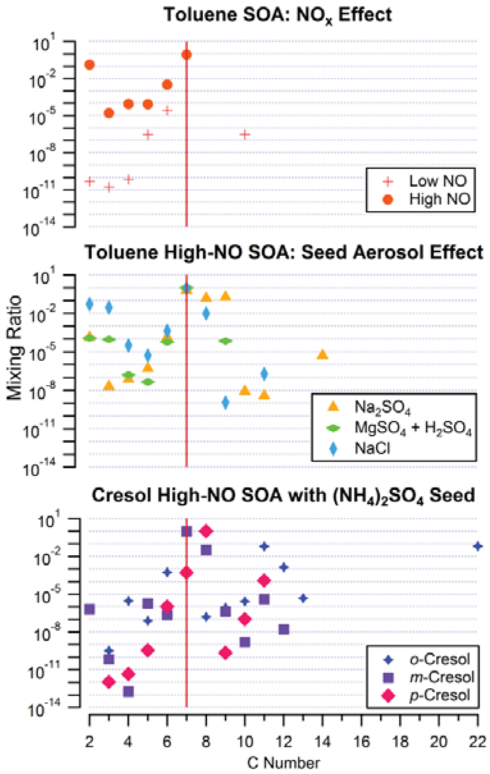

Figure 8. Chemical composition of toluene and cresol SOA, displayed as a function of C number, derived from offline DART-HR-MS analysis. The red line represents the C_7 threshold.

Toluene SOA formed under dry, low- and high-NO conditions with $(NH_4)_2SO_4$ seed comprise high relative mass fractions of highly oxygenated C_7 compounds. The abundance of C_7 oxidation products in toluene SOA suggests the cresol pathway is influential in toluene SOA formation, since fragmentation is a major early-generation mechanism for the bicylic peroxy radical, epoxy muconaldehyde, and toluene peroxy pathways (Figs. 1-4 and 8, and Supporting Information). $C_{10}H_{10}O_4$ is the principal oligomeric species identified in toluene SOA formed under dry low-NO conditions, with a relative mass fraction of 3.0×10^{-5}, and is potentially a hemiacetal formed between a C_7 polyhydroxylated species and a C_3 carbonyl compound. Extensive oligomerization is not found in this case possibly because of the abundance of highly oxidized, bulky, ring-retaining C_7 compounds relative to the modest amount of sub-C_7 compounds.

In the present study, a seed effect is observed in the increased C chain lengths (> C_7) in the presence of Na_2SO_4, $MgSO_4 + H_2SO_4$, and NaCl seeds (Fig. 8). We report here high oligomer C numbers and relative mass fractions in toluene high-NO SOA formed in the presence of Na_2SO_4 (0.34) and NaCl (0.01) seeds relative to that formed in the presence of $MgSO_4 + H_2SO_4$ (7.1×10^{-5}) and $(NH_4)_2SO_4$ (0) seeds. Seed effects have been observed in previous studies as the shifting of oligomer distributions in SOA to higher molecular weights as seed acidity is increased.[6,33] The abundance of lower molecular weight oligomers observed by Gao *et al.* did not change with increased acidity, implying that oligomer types may have different acid sensitivities, which is consistent with observations here.[33] In this study, toluene high-NO SOA has an abundance of polyhydroxylated C_7 species, and these species may have potential to produce an oligomer type that is less responsive to acidic seed. Additionally, the continuity of the oligomer C atom range (C_8, C_9, C_{10}, etc.) suggests that oligomers may be forming between C_7 particle-phase compounds and small gas-phase oxidation products. Hall and Johnston observed the independence of monomer abundance in SOA and monomer vapor pressure and suggested reactive uptake between a monomer colliding and reacting with the particle surface as a potential scenario for oligomer formation in SOA.[50]

In this study, *o*-, *m*- and *p*-Cresol SOA contain abundant oligomeric species (relative mass fractions: 0.13, 0.03, and 0.99, respectively). *o*- and *m*-Cresol-derived oligomeric species have the general forms $C_xH_yO_{4\text{-}5+}$, with < 1% of the oligomeric relative mass fraction composed of $C_xH_yNO_{3\text{-}5+}$ and $C_xH_yO_{2\text{-}3}$. *p*-Cresol SOA contains one identified oligomer, $C_8H_{14}O_7$. The position of the hydroxyl group in the cresol isomer is observed here to affect oligomer formation as well as monomer composition and bulk H:C and O:C trends.

GRAPHICAL ABSTRACT

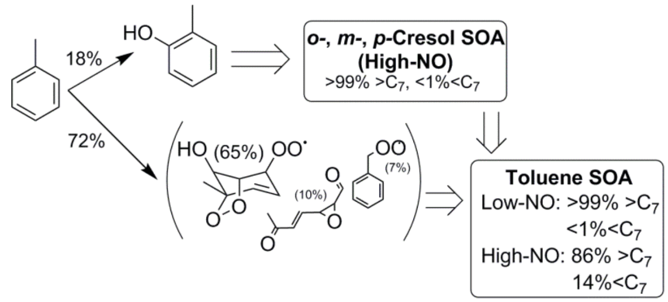

ASSOCIATED CONTENT

Supporting Information. The supporting information includes additional details for the environmental chamber experiments, Master Chemical Mechanisms for non-cresol pathway toluene photooxidation, details on SOA collection by filtration, experimental details from the offline analysis of SOA by DART-HR-MS, tabulated interpreted offline mass spectral data, van Krevelen diagrams of DART-HR-MS and HR-AMS data, details on the qualitative PMF analysis performed in this study and evidence of the solution robustness, as well as HR-AMS data supporting the identification of pyridine and the Chichibabin mechanism for pyridine synthesis.

AUTHOR INFORMATION

Corresponding Author

*Correspondence should be addressed to John H. Seinfeld, seinfeld@caltech.edu.

Author Contributions

The manuscript was written by KAS and JHS. The experiments were performed by KAS, HL, MMC, RHS, and XZ. Data were analyzed by KAS, HL, and MMC.

ACKNOWLEDGMENTS

The authors thank Jill Craven for helpful data discussions and Jeffrey Dake of the United States Army Criminal Investigation Laboratory, Trace Evidence Branch, for experimental assistance with DART-HR-MS analysis. This research was funded by U.S. Department of Energy grant DE-SC 0006626. KAS acknowledges support from a Department of Defense Science, Mathematics, and Research for Transformation Fellowship.

REFERENCES

1. Yu, J.; Jeffries, H. E.; Sexton, K. G. Atmospheric Photooxidation of Alkylbenzenes - I. Carbonyl Product Analyses. *Atmos. Environ.* **1997**, *31*, 2261-2280.

2. Yu, J.; Jeffries, H. E., Atmospheric Photooxidation of Alkylbenzenes – II. Evidence of Formation of Epoxide Intermediates. *Atmos. Environ.* **1997**, *31*, 2281-2287.

3. Calvert, J. G.; Atkinson, R.; Becker, K. H.; Kamens, R. M.; Seinfeld, J. H.; Wallington, T. J.; Yarwood, G. *The Mechanisms of Atmospheric Oxidation of Aromatic Hydrocarbons*; Oxford University Press: New York, 2002.

4. Cao, G.; Jang, M. Effects of Particle Acidity and UV Light on Secondary Organic Aerosol Formation from Oxidation of Aromatics in the Absence of NO_x. *Atmos. Environ.* **2007**, *41*, 7603-7613.

5. Jang, M.; Kamens, R. M. Characterization of Secondary Aerosol from the Photooxidation of Toluene in the Presence of NO_x and 1-Propene. *Environ. Sci. Technol.* **2001**, *35*, 3626-3639.

6. Tolocka, M. P.; Jang, M.; Ginter, J. M.; Cox, F. J.; Kamens, R. M.; Johnston, M. V. Formation of Oligomers in Secondary Organic Aerosol. *Environ. Sci. Technol.* **2004**, *38*, 1428-1434.

7. Jenkin, M. E.; Saunders, S. M.; Wagner, V.; Pilling, M. J. Protocol for the Development of the Master Chemical Mechanism, MCM v3 (Part B): Tropospheric Degradation of Aromatic Volatile Organic Compounds. *Atmos. Chem. Phys.* **2003**, *3*, 181-193.

8. Wagner, V.; Jenkin, M. E.; Saunders, S. M.; Stanton, J.; Wirtz, K.; Pilling, M. J. Modelling of the Photooxidation of Toluene: Conceptual Ideas for Validating Detailed Mechanisms. *Atmos. Chem. Phys.* **2003**, *3*, 89-106.

9. Klotz, B.; Barnes, I.; Becker, K. H.; Golding, B. T. Atmospheric Chemistry of Benzene Oxide/Oxepin. *J. Chem. Soc., Faraday Trans.* **1997**, *93*, 1507-1516.

10. Klotz, B.; Barnes, I.; Golding, B. T.; Becker, K. H. Atmospheric Chemistry of Toluene-1,2-Oxide/2-Methyloxepin. *Phys. Chem. Chem. Phys.* **2000**, *2*, 227-235.

11. Klotz, B.; Sorensen, S.; Barnes, I.; Becker, K. H.; Etzkorn, T.; Volkamer, R.; Platt, U.; Wirtz, K.; Martin-Reviejo, M. Atmospheric Oxidation of Toluene in a Large-Volume Outdoor Photoreactor: In-Situ Determination of Ring-Retaining Product Yields. *J. Phys. Chem. A* **1998**, *102*, 10289-10299.

12. Olariu, R. I.; Klotz, B.; Barnes, I.; Becker, K. H.; Mocanu, R. FT-IR Study of the Ring-Retaining Products from the Reaction of OH Radicals with Phenol, *o*-, *m*-, and *p*-Cresol. *Atmos. Environ.* **2002**, *36*, 3685-3697.

13. Volkamer, R.; Klotz, B.; Barnes, I.; Imamura, T.; Wirtz, K.; Washida, N.; Becker, K. H.; Platt, U. OH-Initiated Oxidation of Benzene: Part I. Phenol Formation under Atmospheric Conditions. *Phys. Chem. Chem. Phys.* **2002**, *4*, 1598-1610.

14. Birdsall, A. W.; Elrod, M. J. Comprehensive NO-Dependent Study of the Products of the Oxidation of Atmospherically Relevant Aromatic Compounds. *J. Phys. Chem. A* **2011**, *115*, 5397-5407.

15. Birdsall, A. W.; Andreoni, J. F.; Elrod, M. J. Investigation of the Role of the Bicyclic Peroxy Radicals in the Oxidation Mechanism of Toluene. *J. Phys. Chem. A* **2010**, *114*, 10655-10663.

16. Baltaretu, C. O.; Lichtman, E. I.; Hadler, A. B.; Elrod, M. J. Primary Atmospheric Oxidation Mechanism for Toluene. *J. Phys. Chem. A* **2009**, *113*, 221-230.

17. Edney, E. O.; Driscoll, D. J.; Weathers, W. S.; Kleindienst, T. E.; Conver, T. S.; McIver, C. D.; Li, W. Formation of Polyketones in Irradiated Toluene/Propylene/NO_x/Air Mixtures. *Aerosol Sci. Technol.* **2001**, *35*, 998-1008.

18. Edney, E. O.; Driscoll, D. J.; Speer, R. E.; Weathers, W. S.; Kleindienst, T. E.; Li, W.; Smith, D. F. Impact of Aerosol Liquid Water on Secondary Organic Aerosol Yields of Irradiated Toluene/Propylene/NO_x/$(NH_4)_2SO_4$/Air Mixtures. *Atmos. Environ.* **2000**, *34*, 3907-3919.

19. Kleindienst, T. E.; Smith, D. F.; Li, W.; Edney, E. O.; Driscoll, D. J.; Speer, R. E.; Weathers, W. S., Secondary Organic Aerosol Formation from the Oxidation of Aromatic Hydrocarbons in the Presence of Dry Submicron Ammonium Sulfate Aerosol. *Atmos. Environ.* **1999**, *33*, 3669-3681.

20. Hildebrandt, L.; Donahue, N. M.; Pandis, S. N. High Formation of Secondary Organic Aerosol from the Photooxidation of Toluene. *Atmos. Chem. Phys.* **2009**, *9*, 2973-2986.

21. Smith, D. F.; McIver, C. D.; Kleindienst, T. E. Primary Product Distribution from the Reaction of Hydroxyl Radicals with Toluene at ppb NO_x Mixing Ratios. *J. Atmos. Chem.* **1998**, *30*, 209-228.

22. Smith, D. F.; Kleindienst, T. E.; McIver, C. D. Primary Product Distributions from the Reaction of OH with *m*- and *p*-Xylene, 1,2,4- and 1,3,5-Trimethylbenzene. *J. Atmos. Chem.* **1999**, *34*, 339-364.

23. Forstner, H. J. L.; Flagan, R. C.; Seinfeld, J. H. Secondary Organic Aerosol from the Photooxidation of Aromatic Hydrocarbons: Molecular Composition. *Environ. Sci. Technol.* **1997**, *31*, 1345-1358.

24. Baltensperger, U.; Kalberer, M.; Dommen, J.; Paulsen, D.; Alfarra, M. R.; Coe, H.; Fisseha, R.; Gascho, A.; Gysel, M.; Nyeki, S.; Sax, M.; Steinbacher, M.; Prevot, A. S. H.; Sjogren, S.; Weingartner, E.; Zenobi, R. Secondary Organic Aerosols from Anthropogenic and Biogenic Precursors. *Faraday Discuss.* **2005**, *130*, 265-278.

25. Cocker, D. R.; Mader, B. T.; Kalberer, M.; Flagan, R. C.; Seinfeld, J. H. The Effect of Water on Gas-Particle Partitioning of Secondary Organic Aerosol: II. *m*-Xylene and 1,3,5-Trimethylbenzene Photooxidation Systems. *Atmos. Environ.* **2001**, *35*, 6073-6085.

26. Nakao, S.; Liu, Y.; Tang, P.; Chen, C. L.; Zhang, J.; Cocker, D. R. Chamber Studies of SOA Formation from Aromatic Hydrocarbons: Observation of Limited Glyoxal Uptake. *Atmos. Chem. Phys.* **2012**, *12*, 3927-3937.

27. Song, C.; Na, K.; Warren, B.; Malloy, Q.; Cocker, D. R. Secondary Organic Aerosol Formation from *m*-Xylene in the Absence of NO_x. *Environ. Sci. Technol.* **2007**, *41*, 7409-7416.

28. Kalberer, M.; Paulsen, D.; Sax, M.; Steinbacher, M.; Dommen, J.; Prevot, A. S. H.; Fisseha, R.; Weingartner, E.; Frankevich, V.; Zenobi, R.; Baltensperger, U. Identification of Polymers as Major Components of Atmospheric Organic Aerosols. *Science* **2004**, *303*, 1659-1662.

29. Kalberer, M.; Sax, M.; Samburova, V. Molecular Size Evolution of Oligomers in Organic Aerosols Collected in Urban Atmospheres and Generated in a Smog Chamber. *Environ. Sci. Technol.* **2006**, *40*, 5917-5922.

30. Sato, K.; Hatakeyama, S.; Imamura, T. Secondary Organic Aerosol Formation During the Photooxidation of Toluene: NO_x Dependence of Chemical Composition. *J. Phys. Chem. A* **2007**, *111*, 9796-9808.

31. Ehn, M.; Thornton, J. A.; Kleist, E.; Sipila, M.; Junninen, H.; Pullinen, I.; Springer, M.; Rubach, F.; Tillmann, R.; Lee, B.; Lopez-Hilfiker, F.; Andres, S.; Acir, I.-H.; Rissanen, M.; Jokinen, T.; Schobesberger, S.; Kangasluoma, J.; Kontkanen, J.; Nieminen, T.; Kurten, T.; Nielsen, L. B.; Jorgensen, S.; Kjaergaard, H. G.; Canagaratna, M.; Dal Maso, M.; Berndt, T.; Petaja, T.; Wahner, A.; Kerminen, V.-M.; Kulmala, M.; Worsnop, D. R.; Wildt, J.; Mentel, T. F. A Large Source of Low-Volatility Secondary Organic Aerosol. *Nature* **2014**, *506*, 476-496.

32. Gao, S.; Keywood, M.; Ng, N. L.; Surratt, J.; Varutbangkul, V.; Bahreini, R.; Flagan, R. C.; Seinfeld, J. H. Low-Molecular-Weight and Oligomeric Components in Secondary Organic Aerosol from the Ozonolysis of Cycloalkenes and α-Pinene. *J. Phys. Chem. A* **2004**, *108*, 10147-10164.

33. Gao, S.; Ng, N. L.; Keywood, M.; Varutbangkul, V.; Bahreini, R.; Nenes, A.; He, J.; Yoo, K. Y.; Beauchamp, J. L.; Hodyss, R. P.; Flagan, R. C.; Seinfeld, J. H. Particle Phase Acidity and Oligomer Formation in Secondary Organic Aerosol. *Environ. Sci. Technol.* **2004**, *38*, 6582-6589.

34. Zhang, X.; Cappa, C. D.; Jathar, S.; McVay, R. C.; Ensberg, J. J.; Kleeman, M. J.; Seinfeld, J. H. Influence of Vapor Wall-Loss in Laboratory Chambers on Yields of Secondary Organic Aerosol. *Proc. Natl. Acad. Sci. USA* **2014**, *116*, 5802-5807.

35. Loza, C. L.; Craven, J. S.; Yee, L. D.; Coggon, M. M.; Schwantes, R. H.; Shiraiwa, M.; Zhang, X.; Schilling, K. A.; Ng, N. L.; Canagaratna, M. R.; Ziemann, P. J.; Flagan, R. C.; Seinfeld, J. H. Secondary Organic Aerosol Yields of 12-Carbon Alkanes. *Atmos. Chem. Phys.* **2014**, *14*, 1423-1439.

36. Aiken, A. C.; De Carlo, P. F.; Kroll, J. H.; Worsnop, D. R.; Huffman, J. A.; Docherty, K. S.; Ulbrich, I. M.; Mohr, C.; Kimmel, J. R.; Sueper, D.; Sun, Y.; Zhang, Q.; Trimborn, A.; Northway, M.; Ziemann, P. J.; Canagaratna, M. R.; Onasch, T. B.; Alfarra, M. R.; Prevot, A. S. H.; Dommen, J.; Duplissy, J.; Metzger, A.; Baltensperger, U.; Jimenez, J. L. O/C and OM/OC Ratios of Primary, Secondary, and Ambient Organic Aerosols with High-Resolution Time-of-Flight Aerosol Mass Spectrometry. *Environ. Sci. Technol.* **2008**, *42*, 4478-4485.

37. Canagaratna, M. R.; Jimenez, J. L.; Kroll, J. H.; Chen, Q.; Kessler, S. H.; Massoli, P.; Hidebrandt Ruiz, L.; Fortner, E.; Williams, L. R.; Wilson, K. R.; Surratt, J. D.; Donahue, N. M.; Jayne, J. T.; Worsnop, D. R. Elemental Ratio Measurements of Organic Compounds Using Aerosol Mass Spectrometry: Characterization, Improved Calibration, and Implications. *Atmos. Chem. Phys. Discuss.* **2014**, *14*, 19791-19835.

38. Craven, J. S.; Yee, L. D.; Ng, N. L.; Canagaratna, M. R.; Loza, C. L.; Schilling, K. A.; Yatavelli, R. L. N.; Thornton, J. A.; Ziemann, P. J.; Flagan, R. C.; Seinfeld, J. H. Analysis of Secondary Organic Aerosol Formation and Aging Using Positive Matrix Factorization of High-Resolution Aerosol Mass Spectra: Application to the Dodecane Low-NO_x System. *Atmos. Chem. Phys.* **2012**, *12*, 11795-11817.

39. Cody, R. B. Observation of Molecular Ions and Analysis of Nonpolar Compounds with the Direct Analysis in Real Time Ion Source. *Anal. Chem.* **2009**, *81*, 1101-1107.

40. Cody, R. B.; Laramee, J. A.; Durst, H. D. Versatile New Ion Source for the Analysis of Materials in Open Air under Ambient Conditions. *Anal. Chem.* **2005**, *77*, 2297-2302.

41. Liu, X.; Jeffries, H. E.; Sexton, K. G. Atmospheric Photochemical Degradation of 1,4-Unsaturated Dicarbonyls. *Environ. Sci. Technol.* **1999**, *33*, 4212-4220.

42. Compernolle, S.; Ceulemans, K.; Müller, J. F., Evaporation: A New Vapour Pressure Estimation Method for Organic Molecules Including Non-Additivity and Intramolecular Interactions. *Atmos. Chem. Phys.* **2011**, *11*, 9431-9450.

43. Nilles, J. M.; Connell, T. R.; Durst, H. D. Quantitation of Chemical Warfare Agents Using the Direct Analysis in Real Time (DART) Technique. *Anal. Chem.* **2009**, *81*, 6744-6749.

44. Schilling Fahnestock, K. A.; Yee, L. D.; Loza, C. L.; Coggon, M. M.; Schwantes, R.; Zhang, X.; Dalleska, N. F.; Seinfeld, J. H. Secondary Organic Aerosol Composition from C_{12} Alkanes. *J. Phys. Chem. A* **2014**, Articles ASAP. http://dx.doi.org/10.1021/jp501779w.

45. Virtanen, A.; Joutsensaari, J.; Koop, T.; Kannosto, J.; Yli-Pirilä, P.; Leskinen, J.; Mäkelä, J. M.; Holopainen, J. K.; Pöschl, U.; Kulmala, M.; Worsnop, D. R.; Laaksonen, A. An Amorphous Solid State of Biogenic Secondary Organic Aerosol Particles. *Nature* **2010,** *467*, 824-827.

46. Bones, D. L.; Reid, J. P.; Lienhard, D. M.; Krieger, U. K. Comparing the mechanism of water condensation and evaporation in glassy aerosol. *Proc. Nat. Acad. Sci. USA* **2012,** *109*, 11613-11618.

47. Chhabra, P. S.; Ng, N. L.; Canagaratna, M. R.; Corrigan, A. L.; Russell, L. M.; Worsnop, D. R.; Flagan, R. C.; Seinfeld, J. H. Elemental Composition and Oxidation of Chamber Organic Aerosol. *Atmos. Chem. Phys.* **2011**, *11*, 8827-8845.

48. Ng, N. L.; Canagaratna, M. R.; Jimenez, J. L.; Chhabra, P. S.; Seinfeld, J. H.; Worsnop, D. R. Changes in Organic Aerosol Composition with Aging Inferred from Aerosol Mass Spectra. *Atmos. Chem. Phys.* **2011**, *11*, 6465-6474.

49. Heald, C. L.; Kroll, J. H.; Jimenez, J. L.; Docherty, K. S.; DeCarlo, P. F.; Aiken, A. C.; Chen, Q.; Martin, S. T.; Farmer, D. K.; Artaxo, P. A Simplified Description of the Evolution of Organic Aerosol Composition in the Atmosphere. *Geophys. Res. Lett.* **2010**, *37*, L08803.

50. Hall, W. A.; Johnston, M. V. Oligomer Formation Pathways in Secondary Organic Aerosol from MS and MS/MS Measurements with High Mass Accuracy and Resolving Power. *J. Amer. Soc. Mass Spectrom.* **2012,** *23*, 1097-1108.